

On the solidification dynamic of an impacted drop

V. Thiévenaz¹, T. Séon^{1†} and C. Josserand²

¹Institut ∂ 'Alembert, UMR 7190, CNRS & Sorbonne Universités, Paris, France

²Laboratoire d'Hydrodynamique (LadHyX), UMR7646 CNRS-Ecole Polytechnique, 91128 Palaiseau CEDEX, France

(Received xx; revised xx; accepted xx)

We investigate experimentally the solidification of a water drop impacting a cold solid substrate. During the initial spreading a thin layer of ice builds, and pins the contact line of the water layer on its edge. The liquid retracts on the ice layer after the time τ_{SCL} , during which the ice layer has grown to reach the thickness h_p . We show that this time is mainly independent of the temperature and of the substrate thermal parameters because it is only due to the relaxation of the water layer contact angle. Using a 1D solidification model, that considers the heat diffusion in the solid and in the ice, coupled with the Stefan condition for the solidification front, we characterize and interpret the thermal dynamics and in particular the diffusion front propagation behaviour. The comparison with our experimental measurements of the frozen drop profiles allows us to determine the thickness of the ice layer h_p that builds during the time τ_{SCL} .

Key words: Drop impact, solidification.

1. Introduction

When a liquid drop is put in contact with a very cold substrate, either by impact or deposition, the freezing of the liquid can lead to surprising final shapes. Understanding the coupling between drop impact and solidification, and the shape of the frozen structure, is in fact crucial in many different contexts and liquids, from airplane icing (Baumert *et al.* 2018) to 3D printing (Derby 2010) and surface metal coating technology (Dhiman *et al.* 2007). Although most of the airplane icing configurations concern impact of ice crystal (Vidaurre & Hallett 2009; Hauk *et al.* 2015), the impact of water droplets on subfreezing substrates can be of great interest in the dynamics of icing formation (Schremb *et al.* 2018). In thermal spray deposition, the geometry of the solidified splat is important for the quality of the coating and depends on the melting of the spray with the substrate (Chandra & Fauchais 2009). Similarly, multiple droplet impacts coupling the fluid dynamics with the solidification thermal processes produce complex splat patterns that determines the coating quality (Dhiman & Chandra 2005). For water, the frozen shape varies from a pointy drop when the drop is simply deposited on the substrate (Snoeijer & Brunet 2012) to irregular pancakes when the drop impacts at high enough velocity (Ghabache *et al.* 2016).

The final shape is thus the result of the coupling between thermal and hydrodynamic processes that both have their own different time scales. Indeed, at short times, we

† Email address for correspondence: thomas.seon@gmail.com

observe a fast free surface deformation of the liquid and its almost immediate adhesion through the formation of a thin layer of ice at the contact of the substrate (Schiaffino & Sonin 1997; de Ruiter *et al.* 2018). At longer time scale, the bulk liquid freezes and the remaining liquid retracts on the growing ice layer (Gao & Sonin 1994; Marin *et al.* 2014). Eventually, because of thermal expansion during the solidification (Wildeman *et al.* 2017) or thermal contraction when the ice becomes cooler (Ghabache *et al.* 2016), the frozen structure can fragment into a myriad of small ice pieces.

In that context, it is important to characterize the thickness of the residual ice layer to understand the stability of the frozen structure (Schremb *et al.* 2018). Indeed, depending on this thickness and the substrate temperature, the frozen structure can remain stick on the substrate or detach through a self-peeling process (Ghabache *et al.* 2016; de Ruiter *et al.* 2018), and the optimal design of the surfaces to avoid icing remains an important open problem (Kreder *et al.* 2016).

In this paper, we investigate experimentally the freezing of a water film formed by the impact of a water drop on cold substrates. We study the growth of the ice from the substrate in order to characterize the thickness properties of the residual ice layer. The paper is organized as follows: Section 2 is a rapid description of the experimental setup and the measurement techniques involved. Section 3 describes the regime when the liquid is out of its wetting equilibrium but remains still and keeps freezing. In Sec. 4 we develop and interpret a model of unidimensional solidification of a liquid on a substrate. Finally, Section 5 presents our experimental results relating to the formation of the residual ice layer.

2. Experimental setup and qualitative description

The classical drop impact setup consists of a syringe pump pushing liquid through a capillary tube from which the drop falls. As the pumping is slow enough, the size of the drop is entirely controlled by the size of the capillary tube. We used two different tubes of inner diameter 1600 μm and 250 μm leading to drop radii $R=1.9$ mm and 1.2 mm or volumes 30 μL and 7 μL respectively. The impact velocity U_0 is controlled by the height of fall. In our case the height of fall H ranges from 15 cm to 45 cm, so that the impact velocity U_0 ranges from 1.7 $\text{m}\cdot\text{s}^{-1}$ to 3 $\text{m}\cdot\text{s}^{-1}$ (following roughly $U_0 = \sqrt{2gH}$). Our substrates are made of blocks (100 \times 100 \times 30 mm) of different materials : steel, copper and marble. Each material having their own thermal parameters : λ the thermal conductivity, C_p the heat capacity and $D = \lambda/\rho C_p$ the heat diffusion coefficient, with ρ the density.

The substrate is placed into a bowl and cooled down by pouring a certain amount liquid nitrogen. The minimal temperature reached in this work is around -80°C . Due to the substrate heat capacity and to the bowl thermal isolation, it takes several hours for the system to warm up to room temperature. The change in the substrate temperature is thus much less than 1°C during the time of an experiment which is roughly 1 second. In order to minimize frost formation, the whole system is set inside a regulated atmosphere chamber which allows us to drastically reduce the humidity. The substrate temperature T_s is measured before each experiment using a surface thermometer. The dynamic of the impact is studied using a high-speed camera, and the height profile of the frozen drop is extracted with a polychromatic confocal sensor (CCS OptimaPlus from STIL Optics) moving along a translation platform.

At room temperature, as a water drop impacts a solid substrate, it spreads, reaches a maximal radius (Laan *et al.* 2014) and immediately starts to retract back to an equilibrium radius (Bartolo *et al.* 2005; Josserand & Thoroddsen 2016). Figure 1 (a)-

(h) shows a sequence of snapshots of a water drop impacting a sub-zero substrate. Here again, the drop spreads rapidly and reaches a maximal spreading diameter (a)-(b). But then the drop does not retract, it is stuck at its maximal diameter (c). This pinning is due to the formation of a thin layer of ice at the substrate/liquid interface during the spreading. On images (c)-(e) the drop is made of a thin layer of ice, attached to the substrate and growing vertically, beneath a thicker layer of water where capillary waves are damping. This remaining water layer is not stable due to its high aspect ratio, so that it still needs to retract in order to reach its equilibrium, and we observe on (e) that the liquid layer actually started to depin from the edge. Then, the liquid retracts on the ice layer (f), until it reaches its typical equilibrium contact angle on ice and forms a spherical-cap-shaped drop (g). Eventually, it completely freezes, yielding a pointy ice drop (Marin *et al.* 2014), on top of an ice pancake (h).

Figure 1 (i) shows the height profile of the frozen drop (h) obtained by scanning the drop diameter using the optical profilometer. This profile shows clearly two different parts: a quasi-cylindrical plate (the so-called ice pancake), whose thickness is denominated as h_p , on top of which we find an ice pattern, consequence of the water retraction.

This structure with an ice pancake in contact with the impacted solid is found anytime a drop impacts a sub-zero cold surface. On the other hand, the ice pattern that is eventually formed above this ice pancake can exhibit different shapes that will be the subject of future works. The ice pancake is in fact crucial in all relevant applications, in particular for the stability of the frozen drop. Indeed, as the temperature of the ice varies, thermal expansion/contraction generates elastic stress that can lead to the delamination of the pancake (de Ruiter *et al.* 2018) or the formation of cracks (Ghabache *et al.* 2016), both being controlled by the thickness h_p . The aim of the present paper is thus dedicated to the quantification of this thickness h_p .

3. The stationary contact line (SCL) regime

A crucial difference with the drop impact at non-freezing temperatures is the existence of a regime in which the contact line seems steady (Fig. 1 (b-e)), before a dewetting transition and the retraction of the water film on the ice layer. It is thus tempting to interpret the thickness of the ice pancake h_p as the ice layer that freezes by thermal conduction during this time. Consequently, in order to validate this idea, we need first to characterize the duration of this regime, that we call stationary contact line (SCL) regime (Rivetti *et al.* 2015). Figure 2 (a) presents the variation of the liquid film radius during an impact, plotted as a function of time, for three different substrate temperatures. The dotted line shows the evolution at room temperature and the two continuous lines at freezing temperature : -14 and -30°C. Without freezing (dotted line) the drop spreads rapidly, reaches its maximal diameter and almost instantaneously retracts. The behavior is different when the drop freezes, after having reached its maximal diameter (illustrated on the curve with the inserts), the stationary contact line regime is observed : the liquid remains attached to the ice layer close to its maximum radius. There, the liquid radius barely varies with time during approximately 60 – 70 ms before the retraction of the liquid film starts. This time between the spreading and the retraction regimes defines the SCL time : τ_{SCL} , as shown on the curves. It appears clearly that the time τ_{SCL} is always much longer than the spreading time (that scales typically as $R/U_0 \sim 1\text{ms}$) so that we will neglect the influence of the spreading dynamics in our theory for the growth of the ice pancake. Finally, we note that the two SCL times, for the two different temperatures, seem to be quite close.

Figure 2(b) shows the dependence of the time τ_{SCL} with the temperature, for different

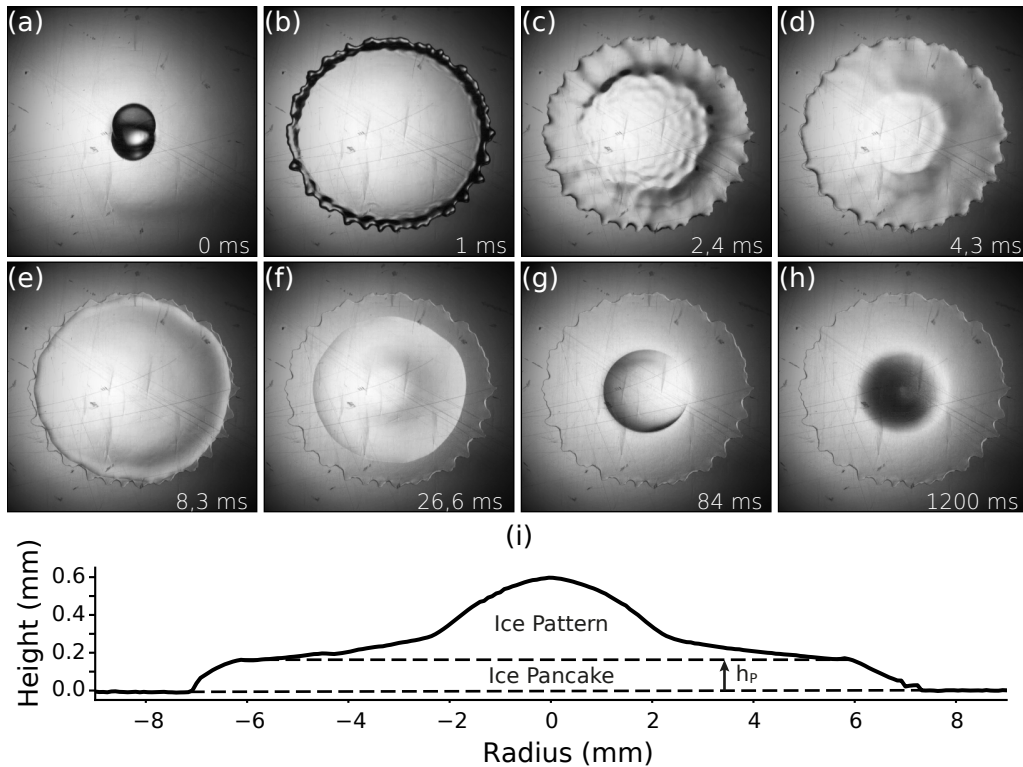


FIGURE 1. Snapshots (a)-(h) show a sequence at different, times indicated on the image, of a drop of water of radius 1.9 mm impacting at velocity $2.6\text{m}\cdot\text{s}^{-1}$ on an aluminium substrate at temperature -9°C . (i) is a height profile of the final frozen pattern, measured using the optical profilometry. The aspect ratio is 20, so the real pattern is much flatter.

heights of fall and same drop size (1.9 mm) and substrate material (steel). Instead of substrate temperature T_s , we use $\Delta T = T_m - T_s$, where T_m is the freezing temperature of the liquid (here for water $T_m = 0^\circ\text{C}$ so that $\Delta T = -T_s$ with the Celsius scale), which is *a priori* the relevant temperature here, because we assume that the energy needed to cool the drop water temperature to the melting one can be neglected (see quantitative argument below). The first observation is that τ_{SCL} reaches a plateau where it is independent of ΔT . The second observation is that the value of this plateau strongly depends on the drop impact velocity and thus on the initial spreading of the liquid film: the larger the maximal diameter at impact, the shorter the liquid layer stays stationary atop the ice pancake before retracting. These two results suggest therefore that τ_{SCL} might be independent of the heat transfert and due to the proper liquid dynamics.

Figure 2(c) presents the variation of τ_{SCL} with ΔT for three different substrates: marble, steel, copper, and two different drop radii on steel substrat (full and empty squares). In each case, the plateau regime is quickly reached confirming this independence of SCL time with ΔT . As expected, the drop size, as the drop impact velocity, seems to play a role in the selection of the plateau value of τ_{SCL} . What is more surprising here is the variation of the plateau value with the substrate material: τ_{SCL} decreases as the substrate thermal conductivity increases. This appears as a contradiction with the previous result that τ_{SCL} does not depend on the substrat temperature and, thus, seems to be independent of the thermic parameters!

To explain the existence of this delay τ_{SCL} , between spreading and retraction when

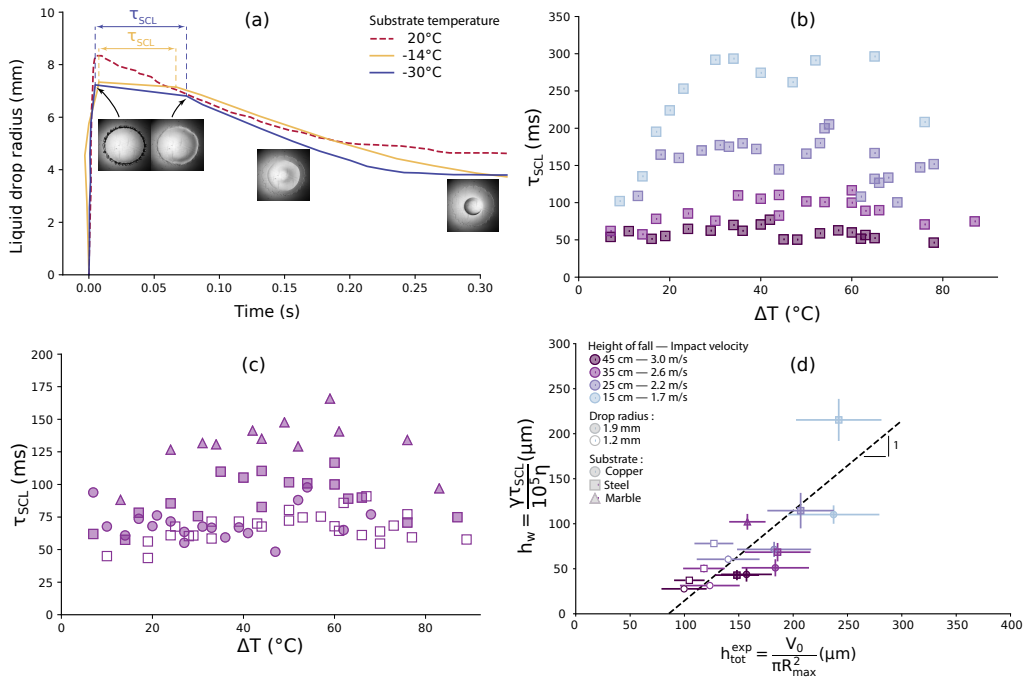


FIGURE 2. (a) The dynamic of spreading and retraction of the drop. The radius of the liquid film is plotted as function of time. Inset pictures show the aspect of the film on the different stages. On all the following graphs, impact velocities are represented by colors (light blue for the slowest to dark purple for the fastest), substrate by symbols (circles for copper, squares for steel and triangles for marble) and drop radii by the filling (full symbols for $R = 1.9\text{mm}$, empty symbols for $R = 1.2\text{mm}$). (b) τ_{SCL} as a function of the temperature ΔT for different impact velocities. The drop radius is 1.9mm and the substrate is steel. (c) τ_{SCL} as a function of the temperature ΔT for different substrates. The impact velocity is 2.6 m/s and the drop radius is 1.9mm (full symbols). Results for a drop of $R = 1.2\text{mm}$ impacting on steel at the same velocity are shown with empty squares. (d) Theoretical prediction for the water film thickness h_w as a function of its experimental estimation h_{tot}^{exp} . Each point represents a series experiments with given impact velocity, substrate and drop radius. The error bars contain the variations within each series. The dashed line is a linear fit with the slope set to one.

water freezes we will use an argument of the previous work of Rivetti *et al.* (2015) on the relaxation of a contact line pinned at the edge of a polymer film. Similarly, we assume here that, in the SCL regime, the time τ_{SCL} is due to the relaxation dynamics of the contact angle θ formed by the liquid film on top of the growing ice pancake and pinned at its edge. The initial angle is given by the spreading dynamics (influenced by the drop impact velocity, the substrate wetting angle, and the drop size), and eventually, the receding motion of the line starts when the angle reaches a critical value enabling the depinning of the contact line. In the experiment of Rivetti *et al.* (2015), this angle is $\theta^* = 4.5^\circ \pm 0.5^\circ$ and surprisingly appears to be independent of the liquid parameter and film thickness. Moreover, because the liquid film is very thin, its dynamics can be taken in the lubrication regime so that the contact line relaxation follows a self-similar evolution leading to a relaxation time $t_w \propto (h_0 \eta) / \gamma$ with the proportional coefficient function of θ^* , being about 10^5 in their experiments. Finally, as soon as the contact line retracts, they showed that θ increases to a receding contact angle which stays roughly constant during dewetting. In order to show that the same dynamics is at play in our experiments, we compare on figure 2(d) the thickness h_w of the liquid film that would correspond to the

relaxation time τ_{SCL} following this self-similar dynamics (*i.e.* $h_w = \gamma\tau_{\text{SCL}}/(10^5\eta)$) with the thickness of the water film $h_{\text{tot}}^{\text{exp}}$ formed at the end of the spreading, neglecting ice formation ($h_{\text{tot}}^{\text{exp}} = V_{\text{tot}}/\pi R_{\text{max}}^2$ with V_{tot} the total volume of the drop). Remarkably, the experimental data gather along a line of slope 1 suggesting that this relaxation scenario of the the contact line is correct. We have used for comparaison the same value of θ^* than for the polymer films (leading to the 10^5 prefactor for h_w), while there is no reason that this value is pertinent for water films. In fact, when trying to fit the best linear fit for the data of figure 2(d), we found an angle slightly different but with no significant improvement when comparing with the θ^* correlation, so that we have kept this value for the sake of simplicity. The fact that this dewetting angle θ^* appears to be almost independent on the substrates, the liquids and the film thicknesses while our experiments and those of Rivetti *et al.* (2015) concern film with totally different thickness (from hundreds of micrometers here to hundreds of nanometer there) is a very interesting and intriguing result, that might shed light on an universal dewetting mechanism that should deserve specific investigations in the future. Remarkably, since $h_{\text{tot}}^{\text{exp}}$ has been taken as the total height, it is the sum of the ice pancake height and the water film so that the intersection of the dotted line with the x-axis gives a consistent estimation of the ice pancake thickness. Finally, following these results, the stationary contact line time (τ_{SCL}) varies linearly with the thickness of the liquid pancake at impact ($h_{\text{tot}}^{\text{exp}}$). As the spread drop diameter increases with the impact velocity, the liquid pancake is thinner and we understand why τ_{SCL} decreases when the impact velocity increases (Fig. 2 (b)). These results resolve also the contradiction that we draw concerning the dependance of τ_{SCL} with the substrate while it does only slightly depend on the temperature. The contact angle relaxation dynamics suggests indeed that the substrate intervenes through its wetting properties that influences the spreading radius and therefore the liquid film thickness pinned on the thin ice layer. In this scenario, the thermal properties of the substrate plays (almost) no role, explaining thus the (almost) independence of τ_{SCL} with the temperature.

4. Unidimensional solidification model

During the SCL regime, the droplet is constantly cooled down by the substrate so that the ice layer keeps growing from the substrate and the final pancake thickness h_p is likely to be linked with the thickness of the ice layer built during this time τ_{SCL} . In that purpose, we introduce in this section a simplified 1-D model that will characterize the main properties of the solidification dynamics involved here. Our starting configuration is at the end of the rapid spreading dynamics, where we consider that a very thin ("infinitely thin" in the model) layer of ice has formed during the spreading due to the sudden contact of the liquid with the cold substrate. This layer of ice will then be growing during the SCL regime. The subsequent configuration is thus a solid substrate in contact with an ice layer growing in water (see schematic Fig.3 (a)). This dynamic of solidification is reminiscent of the so-called Stefan problem, widely explored as the generic problem of a discontinuous flux at a moving interface (Stefan 1891; Gupta 2003). The Stefan problem however usually concerns only the dynamics of the front separating the two phases (in general liquid and solid) of the same material, with different thermal properties. It assumes semi-infinite phases, which is not coherent with the case of a drop impacting a cold substrate since the ice and the water layers are rather thin. When a solid body is added, the problem becomes more complex. For instance, considering the temperature of the solid to be constant and thus acting only as a fixed temperature boundary condition, leads already to a transcendental equation for the solidification front dynamics (Worster 2000). But in fact, the substrate temperature cannot be taken constant (the drop is heating the

substrate) and thermal properties of the material have to be considered (de Ruiter *et al.* 2018).

The choice of a one-dimensional model is supported by the strong aspect ratio of the drop which resembles a pancake much more than a spherical cap (see Fig.1). In addition, we will assume that the liquid is at the melting temperature T_m . This approximation can be justified both by, again, the small thickness of the liquid layer and, by the low energy needed to cool the water down to the melting temperature ($C_{pl}(T_d - T_m) \sim 4000 \times 20 \sim 8 \cdot 10^4 \text{ J}\cdot\text{kg}^{-1}$, where C_{pl} is the heat capacity of water and T_d the initial temperature of the drop), compared to the latent heat for solidification ($L \sim 3 \cdot 10^5 \text{ J}\cdot\text{kg}^{-1}$). We end up with heat equations for the temperature field $T(z, t)$ in the substrate (for $z \leq 0$) and in the ice layer (defined by $0 \leq z \leq h(t)$, where $h(t)$ is the thickness of the ice layer) and a constant temperature T_m in the liquid ($z > h(t)$):

$$\frac{\partial T}{\partial t} = D_s \frac{\partial^2 T}{\partial z^2} \quad \text{for } z \leq 0; \quad \frac{\partial T}{\partial t} = D_i \frac{\partial^2 T}{\partial z^2} \quad \text{for } 0 \leq z \leq h(t) \quad (4.1)$$

where $D_{s,i}$ are the heat diffusion coefficients in the substrate and the ice respectively. These equations have to be solved with regards to the following boundary conditions at the two interfaces, firstly $z = 0$:

$$T(0^-, t) = T(0^+, t); \quad \lambda_s \frac{\partial T}{\partial z}(0^-, t) = \lambda_i \frac{\partial T}{\partial z}(0^+, t). \quad (4.2)$$

These conditions impose both the continuity of the temperature and the heat flux at the solid/ice interface, $\lambda_{s,i}$ being the thermal conductivity of the substrate material and the ice respectively. For $z = h(t)$, we have:

$$T(h(t)^-, t) = T_m; \quad \lambda_i \frac{\partial T}{\partial z}(h(t)^-, t) = \rho_i L \frac{dh}{dt}. \quad (4.3)$$

which corresponds to the continuity of the temperature again, and the Stefan condition at the solidification front. The Stefan condition imposes here that the water-ice phase change releases a heat flux into the ice. Finally, we impose also a boundary condition for the substrate temperature far from the interface:

$$\lim_{z \rightarrow -\infty} T(z, t) = T_s, \quad (4.4)$$

and we complement this set of equations by the initial conditions taken at $t = 0$:

$$T(z, 0) = T_s \quad \text{for } z \leq 0 \quad \text{and} \quad h(0) = 0, \quad (4.5)$$

indicating that at $t = 0$ the solid and the liquid are suddenly in contact. To the best of our knowledge, we are not aware of such system of equations modeling ice growth by a sudden contact between a liquid and a solid substrate. In fact, multilayer heat transfers with solidification/fusion have been considered numerically in the case of laser heating of nanoscale metal films, leading to similar set of equations, but with different boundary/initial conditions (Font *et al.* 2017).

Similarity analysis shows that this diffusive problem exhibits a self-similar behavior, with the usual self-similar variable involved in diffusion problems $\eta = \frac{z}{\sqrt{t}}$, even in the presence of the moving solidification front. In this case, the solidification follows the usual diffusive front growth law :

$$h(t) = \sqrt{D_{\text{eff}} t} \quad (4.6)$$

where D_{eff} is the effective diffusion coefficient that determines the growth of the ice layer. It is really the quantity of interest that we need to compute and thus relate to the different thermal properties of our problem.

Introducing the self-similar variable in the set of Equations (4.1)–(4.5), we obtain the following solutions for the temperature field:

$$T(z, t) = T_0 + (T_0 - T_s) \cdot \text{Erf} \left(\frac{z}{2\sqrt{D_s t}} \right) \text{ for } z \leq 0 \text{ and} \quad (4.7)$$

$$T(z, t) = T_0 + \frac{e_s}{e_i} (T_0 - T_s) \cdot \text{Erf} \left(\frac{z}{2\sqrt{D_i t}} \right) \text{ for } 0 \leq z \leq h(t) \quad (4.8)$$

where $e_{s,i} = \sqrt{\lambda_{s,i} \rho_{s,i} C_{ps,i}}$ are the effusivities of the materials and T_0 , the temperature at the ice/substrate interface (a constant in time in this self-similar framework) is an integration constant to be determined by the boundary conditions. The error function, Erf is defined by:

$$\text{Erf}(x) = \frac{2}{\sqrt{\pi}} \int_0^x e^{-\xi^2} d\xi. \quad (4.9)$$

Then, by imposing the Stefan condition at $z = h(t)$ (eqs. 4.3), we obtain the following transcendental equation:

$$\text{St} = \frac{\sqrt{\pi\beta}}{2} e^{\frac{\beta}{4}} \left(\frac{e_i}{e_s} + \text{Erf} \left(\frac{\sqrt{\beta}}{2} \right) \right) \quad (4.10)$$

that links St, the Stefan number, with the ratio of the diffusion coefficients β , defined respectively by:

$$\text{St} = \frac{C_{pi} \Delta T}{L} \text{ and } \beta = \frac{D_{\text{eff}}}{D_i} \quad (4.11)$$

From the relation (4.10) it is easy to deduce the asymptotic behaviours for small and large Stefan numbers:

$$\beta \sim \frac{4e_s^2}{\pi e_i^2} \text{St}^2 \text{ for } \text{St} \ll 1, \quad \text{and} \quad \beta \sim 4 \ln(\text{St}) \text{ for } \text{St} \gg 1. \quad (4.12)$$

An interesting physical quantity to compute is the dimensionless ice/substrate interface temperature \bar{T}_0 yielding:

$$\bar{T}_0 = \frac{T_0 - T_s}{T_m - T_s} = \frac{1}{1 + \frac{e_s}{e_i} \text{Erf} \left(\frac{\sqrt{\beta}}{2} \right)} \quad (4.13)$$

such that \bar{T}_0 varies between 0 and 1 with $\bar{T}_0 = 0$ for $T_0 = T_s$ and $\bar{T}_0 = 1$ for $T_0 = T_m$ (see schematic Fig.3 (a)). Then from the asymptotic relations between β and St (Eqs. 4.12), we obtain that $T_0 \rightarrow T_m$ for small Stefan numbers while it converges to an intermediate temperature for large Stefan number:

$$\lim_{\text{St} \rightarrow \infty} T_0 = T_s + (T_m - T_s) \frac{1}{1 + \frac{e_s}{e_i}}, \quad (4.14)$$

which corresponds to the interface temperature when two infinite medium are suddenly put in contact (de Ruiter *et al.* 2018).

In order to further understand how the ice layer grows and which thermal fields are formed in the substrate and the ice layer, we will study the normalized temperature profiles:

$$\bar{T}(z, t) = \frac{T(z, t) - T_s}{T_m - T_s}$$

for different values of the Stefan number and for the three different materials used here.

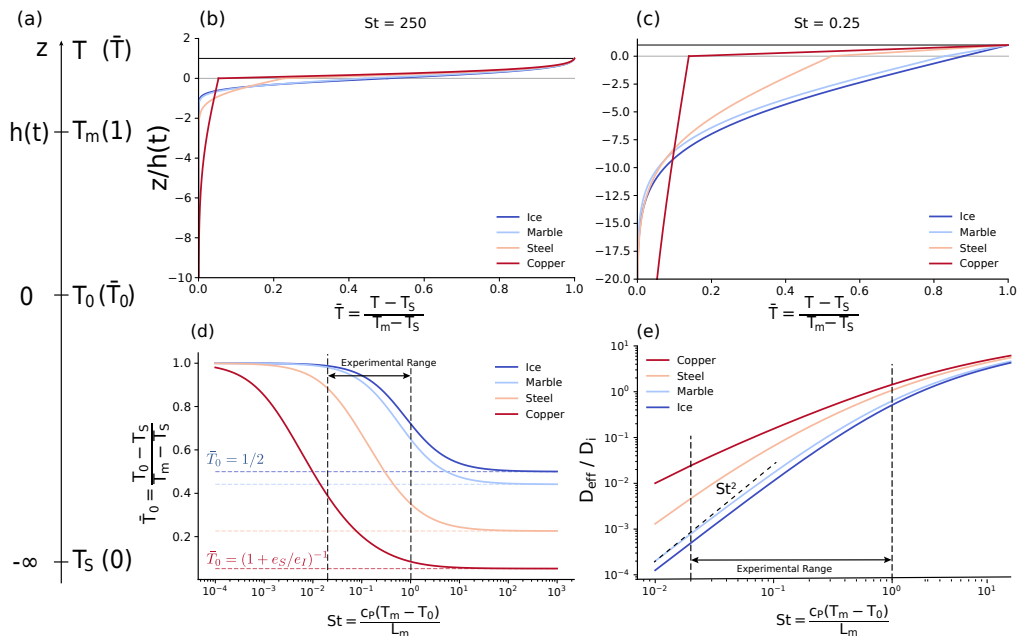


FIGURE 3. Results of the model for the different substrates (copper: red, steel: orange, marble: light blue) and ice (dark blue) that is for comparison with the Stefan problem with infinite ice and infinite liquid water. (a) Schematic of the problem with its boundary conditions in $z = h(t)$ and $z = -\infty$. (b) & (c): Dimensionless temperature profiles $\bar{T}(z, t) = \frac{T(z, t) - T_s}{T_m - T_s}$ as function of the rescaled vertical variable $z/\sqrt{D_{\text{eff}}t}$, obtained from eq. 4.8 and 4.7 for two characteristic Stefan number $St = 250$ (b) and $St = 0.25$ (c). (d) Dimensionless contact temperature, obtained from eq. 4.13. Regardless of the substrate, it goes from 1 for $St \rightarrow 0$ to the asymptotical values $(1 + e_s/e_i)^{-1}$ (indicated on the figure) when $St \rightarrow \infty$, reminiscent of the contact temperature of two infinite bodies initially at different temperatures. (e) The effective diffusion coefficient of the solidification front normalized by the thermal diffusion coefficient of the ice, $\beta = D_{\text{eff}}/D_i$, as a function of the Stefan number. The differences between substrates are more important at low Stefan number, and the asymptotic regime at low Stefan number $\beta \propto St^2$ is indicated (dashed line). For these two last figures (c) and (d), the present experimental temperature range is represented on the graphs.

In particular, two specific values of the Stefan number have been chosen to exhibit some peculiar behavior, respectively a large value $St = 250 \gg 1$ (figure 3(b)) and a value of order one $St = 0.25 \sim 1$ (figure 3(c)). The "continuous" case where ice with the temperature T_s is used as a substrate has been added for comparison. Note that for our configuration, the case $St = 250$ is unphysical since it would correspond to a substrate temperature $T_s = -40000^\circ\text{C}$, far below the absolute zero! On the other hand, the case $St = 0.25$ is within our experimental temperature range since it corresponds to $T_s = -40^\circ\text{C}$. The profiles evolve thus in figures 3(b) and (c) from the substrate temperature T_s ($\bar{T}(z \rightarrow -\infty, t) = 0$) up to the solidification temperature $T_m = 0^\circ\text{C}$ ($\bar{T}(h(t) = \sqrt{D_{\text{eff}}t}, t) = 1$). The vertical position is normalized by the thickness of the growing ice layer ($z/\sqrt{D_{\text{eff}}t}$), showing that the thermal diffusive layer in the substrate is several times thicker than the ice layer except for large Stefan number when the substrate is precisely ice. The case $St = 250$ (b) describes the high Stefan numbers regime where the temperature profiles exhibit the shape of the error function (4.9) within both the ice and the substrate domains. The temperature gradient is then discontinuous

at the contact between the ice and the substrate ($z=0$), because of the discontinuity of the thermal conductivities. For $St = 0.25$ (b), which falls within the temperature range of our experiments, the temperature profile tends to be linear in the ice while it still exhibits an error function profile in the substrate. In addition, figures 3 (d) and (e) present respectively the normalized temperature \bar{T}_0 (Eq. 4.13) and the normalized effective diffusion coefficient $\beta = D_{\text{eff}}/D_i$ (Eq. 4.6), plotted as functions of the Stefan number, for the three different materials used in our experiment, and for an ice substrate. Remember that increasing the Stefan number corresponds to decrease the substrate temperature. The experimental temperature range is represented on the graphs, between around $St = 10^{-2}$ which corresponds roughly to a 1°C temperature difference between the substrate and the front, and $St = 1$ which corresponds to a temperature difference close to a hundred.

In our system, the thermal dynamics is controlled by two different energy sources ; the heat released by the solidification, which can be estimated as follow (per unit surface) :

$$\int_0^t \rho_i L \left(\frac{dh}{dt} \right) dt = \rho_i L \sqrt{D_{\text{eff}} t} \sim St \rho_i L \sqrt{D_i t}$$

and the heat released by cooling down the ice, estimated using eq. 4.12 as :

$$\rho_i C_{pi} \Delta T h(t) = \rho_i C_{pi} \Delta T \sqrt{D_{\text{eff}} t} \sim St \rho_i C_{pi} \Delta T \sqrt{D_i t} = St^2 \rho_i L \sqrt{D_i t}.$$

To better understand the different regimes observed in the figures 3, we can investigate the two asymptotic behaviours of our model: the solidification dominated regime ($St \ll 1$) and the ice cooling dominated ($St \gg 1$). Let us first consider the latter theoretical case of large Stefan numbers that corresponds to $C_{pi} \Delta T \gg L$, meaning that the latent heat L released by the solidification at the water/ice interface $z = h(t)$, is negligible compared to the heat energy released by cooling the ice ($C_{pi} \Delta T$) from the melting temperature T_m to the substrate one T_s . In this case, the ice growth, characterized by the effective diffusion coefficient D_{eff} (figure 3(e)), and the substrate, are almost independent from each others. It can be seen from eq. 4.10 in the large Stefan number limit: the substrate is almost not warmed up by the solidification and does not influence the front propagation. As a consequence, the dynamics is dominated by the self-similar variation of the temperature profiles with time; they exhibit two Erf function that join at the ice/substrate interface (Fig. 3 (b)). If the diffusive coefficients in the ice and the substrate are the same, which is the case when the substrate is ice and almost the case when the substrate is marble, the Erf shape of the temperature profile are symmetrical with respect to $z = 0$. In other cases (steel and copper), this symmetry of the error function is broken. In this limit, the temperature of the ice/substrate interface is the asymptotic limit given by the equation 4.14 (Fig. 3 (d)). In the particular case where the substrate is ice, this interface temperature is exactly the mean value between T_m and T_s : $T_0 = \frac{1}{2}(T_m + T_s)$. Finally, figure 3 (e) shows that in this theoretical limit ($St \gg 1$), the front propagation dynamics is not much influenced by the substrate thermal conductivity as all the substrates gather on the ice curve.

On the other hand, in the opposite limit ($St \ll 1$), the latent heat released by the solidification is much larger than the heat released by cooling the ice down to T_s . The heat released by the ice is thus negligible compared to the one released by the solidification, indicating that the heat reaching the substrate comes mainly from the ice/water interface. The ice layer is inert in the sense that it only transfers the heat flux coming from the solidification to the substrate: the heat flux stays constant through the ice layer. This explains why the temperature field is linear in the ice (Fig. 3 (c)). The slope is selected

by the front dynamics and evolves slowly with time:

$$\lambda_i \partial_z T = \rho_i L \frac{dh}{dt} = \frac{1}{2} \rho_i L \sqrt{\frac{D_{\text{eff}}}{t}} \sim \text{St} \rho_i L \sqrt{\frac{D_i}{t}}.$$

This linear profile in the ice joins an Erf profile in the substrate which goes deeper (relatively to $h(t)$) compared to the large Stefan regime. The freezing process is efficient enough to warm the substrate up. This explains why the interface temperature T_0 increases (Fig. 3(d)) and tends toward T_m ($T_0 \rightarrow T_m$ for $St \rightarrow 0$ (eq. 4.13)), following:

$$\frac{T_m - T_0}{T_m - T_s} = 1 - \bar{T}_0 \sim \frac{e_s}{e_i} \text{Erf} \left(\frac{\sqrt{\beta}}{2} \right) \sim \frac{e_s}{e_i} \text{St}.$$

Finally, the effective diffusion coefficient is smaller than in the large Stefan regime (Fig. 3 (e)). This can be understood easily since decreasing the Stefan number corresponds to warming the substrate up, so the ice grows slower. In this regime we observe that all the curves follow $D_{\text{eff}} \sim \text{St}^2 D_i$ as by eq. (4.12). What is very interesting is that D_{eff} for metal substrates differs by several orders of magnitude from the one of the ice. Indeed, as the Stefan number decreases, the ice gets more and more inert, and the solidification front propagation becomes more and more influenced by the substrate thermic parameters. In this case, the higher the substrate thermal conductivity, the faster the solidification front propagation (see eq. 4.12).

5. The ice pancake

At this point, we know the time during which the ice pancake is building (τ_{SCL}) and we have a model for the ice growth (D_{eff}); we now need the experimental thickness of the pancake (h_p). Figures 4(a)-(c) show the experimental measurement of h_p deduced from the height profiles of the frozen drops (see Fig. 1(i)), as a function of ΔT , respectively for four different drop impact velocities (a), three different substrates (b) and two different drop sizes (c). These control parameters, and their corresponding markers, are the same as those used in figure 2.

These figures show that the underlying ice layer becomes thicker when: i) substrate is colder (Fig. 4 (a), (b) and (c)); which is expected since more liquid can be frozen during the solidification time that appeared to be mostly constant with ΔT (Fig. 2(b) and (c)). ii) The substrate heat conductivity increases (Fig. 4(b)): the heat is indeed transferred to the substrate with higher efficiency, so that the freezing front can propagate faster during a solidification time that, again, does not vary much (Fig. 2(d)). iii) The drop impact velocity is slower (Fig. 4(a)), or the drop size is smaller (Fig. 4(c)), because the spread drop stays freezing longer before retracting (Fig. 2(b) and (c)).

We can now compare these experimental results to our model. Figure 4 (d) presents the variation of h_p^2/τ_{SCL} , which represents the experimental diffusion coefficient of the solidification front, as a function of the effective diffusion coefficient D_{eff} determined by our model, for all the substrate materials, substrate temperatures, drop sizes and impact velocities investigated experimentally. We observe a nice collapse of all the data into a straight line. This indicates clearly that our simplified 1D model account well for this problem and that the ice pancake formation is controlled by the thermal diffusion during the depinning time of the remaining liquid film.

The collapsed data lie along a line with a slope of 1.8, represented by a dashed line above the dotted line of slope 1. We can therefore conclude that the ice pancake thickness

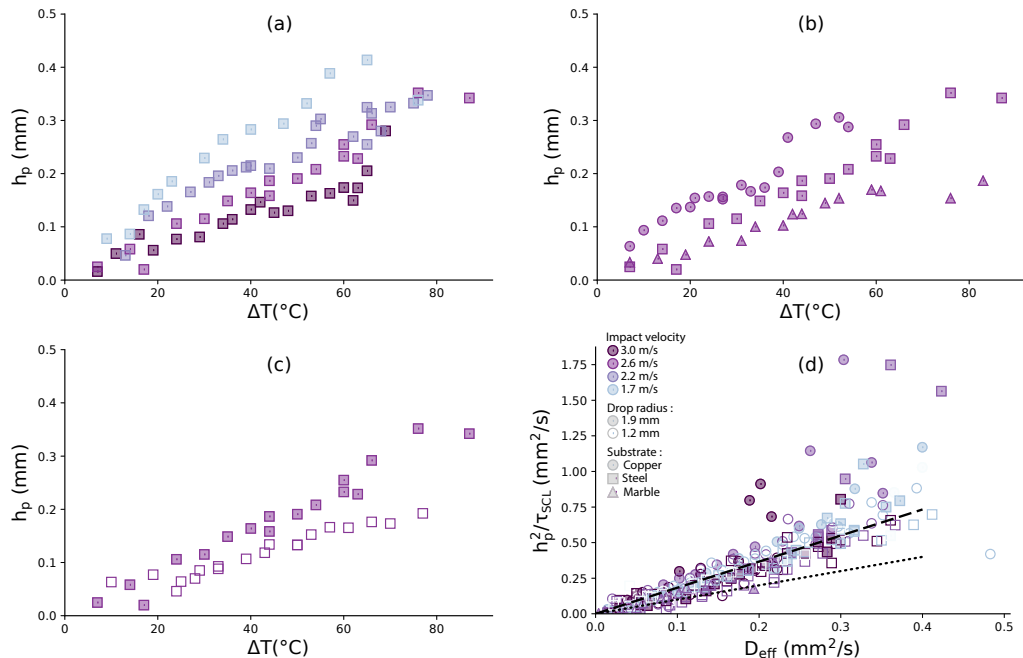


FIGURE 4. (a) Evolution of the underlying ice plate thickness h_p as a function of the temperature ΔT for different impact velocities, on the same substrate (steel) and with the same drop radius (1.9 mm). The colder the substrate is, the thicker the ice layer is. For a given temperature the ice layer is thinner for the highest impact velocities. (b) Evolution of h_p along ΔT , for different substrates, with the same impact velocity (2.6 m/s) and drop radius (1.9 mm). For a given temperature, the more conductive the substrate, the thicker the ice layer. (c) Evolution of h_p with ΔT for different drop radius, on the same substrate (steel) and at the same velocity (2.6 m/s). The smaller the drop the less it freezes. (d) Rescaling of the measurements against the model: the measured diffusivity and the solidification front, h_p^2/τ_{SCL} is plotted against the effective diffusion coefficient obtained through the previously described model (Eq. 4.6 and 4.10). The thick dashed line is a linear fit of the data points, showing a slope of 1.8. The thin dashed line has a slope 1 as predicted by the model.

is well described by the expression :

$$h_p^2 \simeq 1.8 D_{eff} \tau_{SCL}$$

The slightly greater than one pre-factor indicates that the actual growth of the ice layer is faster than what our model predicts – in other words, the thermal transfer in our experiment is more efficient than in the 1D model. This might be due to the three-dimensional shape of the freezing drop which is not taken into account in the one-dimensional model. In the 3D case, the drop will have a finite radius while the substrate has a much larger lateral extension, so that radial diffusion in the substrate can add up to vertical diffusion and speed up the whole process of freezing.

We observe that some experiments are not collapsing on the line with the others. They appear particularly for an effective diffusive coefficient greater than 2.10^{-7} m²/s. This limit of our model probably comes from the hypothesis of semi-infinite water in the freezing model. Indeed, if we estimate the thickness of the freezing water film h_f with the drop volume V_0 and the spreading radius R_{max} , we find $h_f \sim V_0/\pi R_{max}^2$. With a drop of volume $V_0 = 30 \mu\text{L}$ spreading to a radius of $R_{max} = 7 \text{ mm}$, we obtain $h_f \sim 200 \mu\text{m}$ which

corresponds to highest values of h_p . Thus, if almost the whole film freezes during τ_{SCL} , the hypothesis of semi-infinite water does not hold anymore.

6. Conclusion

By studying precisely the freezing of a drop impacting a cold substrate, we have shown that the dynamics could be decomposed in four phases. A rapid spreading of the drop that ends with a very thin ice layer on top of which a liquid water layer is pinned. A still period during which the water layer is almost at rest, and while the ice layer is growing by thermal exchange, the contact angle of the liquid layer is relaxing. Then, after the time τ_{SCL} , when the contact angle has reached a critical value retraction, the water film retracts on the ice layer until it reaches an equilibrium. The last phase consist of the freezing of the remaining liquid forming the final ice pattern. The paper is devoted to the characterization of the thermal dynamics during the second phase time τ_{SCL} when the contact line is steady. Our goal is to determine the subsequent thickness of the ice pancake, h_p .

We have observed that, over a large range of temperature, τ_{SCL} is independent of the temperature and of the substrate thermal parameters, proving that this phase is controlled by the contact angle relaxation. Therefore, we have shown that τ_{SCL} can be roughly expressed by the unique expression :

$$\tau_{\text{SCL}} = 10^5 \frac{\eta}{\gamma} \left(70 + \frac{V_0}{\pi R_{\text{max}}^2} \right)$$

We have then developed a unidimensional solidification model that considers the heat diffusion in the solid and in the ice coupled with the Stefan condition for the solidification front. This leads to a the characterization of the diffusion front dynamics, that involves the effective diffusion coefficient D_{eff} . Using this model, we provide a general expression for the ice pancake thickness :

$$h_p^2 \simeq 1.8 D_{\text{eff}} \tau_{\text{SCL}} = 1.8 \cdot 10^5 D_{\text{eff}} \frac{\eta}{\gamma} \left(70 + \frac{V_0}{\pi R_{\text{max}}^2} \right)$$

that accounts quantitatively for almost all of our experiments. This quantity h_p has many practical interests since it provides an estimate of the splat thickness formed by the impact. Controlling this thickness is thus crucial for coating and 3D printing technology (Derby 2010) and for the adhesion stability of the splat (de Ruiter *et al.* 2018). Our work provides therefore a general framework to model and study more complex configuration such as multiple drops impacts for airplane icing or spray coating (Chandra & Fauchais 2009) for instance.

REFERENCES

- BARTOLO, DENIS, JOSSERAND, CHRISTOPHE & BONN, DANIEL 2005 Retraction dynamics of aqueous drops upon impact on non-wetting surfaces. *J. Fluid Mech.* **545**, 329–338.
- BAUMERT, A., BANSMER, S., TRONTIN, P. & VILLEDIEU, P. 2018 Experimental and numerical investigations on aircraft icing at mixed phase conditions. *Int. J. Heat Mass Transf.* **123**, 957–978.
- CHANDRA, S. & FAUCHAIS, P. 2009 Formation of solid splats during thermal spray deposition. *J. Thermal Spray Tech.* **18**, 148–180.
- DERBY, B. 2010 Inkjet printing of functional and structural materials: fluid property requirements, feature stability and resolution. *Annu. Rev. Mater. Res.* **40**, 395–414.
- DHIMAN, R. & CHANDRA, S. 2005 Freezing-induced splashing during impact of molten metal droplets with high weber numbers. *Int. J. Heat Mass Transf.* **48**, 5625–5638.

- DHIMAN, R., DONALD, A.G. MAC & CHANDRA, S. 2007 Predicting splat morphology in a thermal spray process. *Surf. Coat. Technol.* **201**, 7789–7801.
- FONT, F., AFKHAM, S. & KONDIC, L. 2017 Substrate melting during laser heating of nanoscale metal films. *Int. J. Heat Mass Transf.* **113**, 237–245.
- GAO, FUQUAN & SONIN, AIN A 1994 Precise deposition of molten microdrops: the physics of digital microfabrication. In *Proc. R. Soc. Lond. A*, , vol. 444, pp. 533–554. The Royal Society.
- GHABACHE, ELISABETH, JOSSERAND, CHRISTOPHE & SÉON, THOMAS 2016 Frozen impacted drop: From fragmentation to hierarchical crack patterns. *Physical Review Letters* **117** (7), 074501.
- GUPTA, S.C. 2003 *The Classical Stefan Problem - Basic Concepts, Modelling and Analysis*. Elsevier Science B.V, Amsterdam.
- HAUK, T., BONACCURSO, E., ROISMAN, I.V. & TROPEA, C. 2015 Ice crystal impact onto a dry solid wall. particle fragmentation. *Proc. R. Soc. A* **471**, 20150399.
- JOSSERAND, C & THORODDSEN, ST 2016 Drop impact on a solid surface. *Annual Review of Fluid Mechanics* **48**, 365–391.
- KREDER, M.J., ALVARENGA, J., KIM, P. & AIZENBERG, J. 2016 Design of anti-icing surfaces: smooth, textured or slippery? *Nature Reviews Materials* **1**, 1–15.
- LAAN, NICK, DE BRUIN, KARLA G, BARTOLO, DENIS, JOSSERAND, CHRISTOPHE & BONN, DANIEL 2014 Maximum diameter of impacting liquid droplets. *Physical Review Applied* **2** (4), 044018.
- MARIN, ALVARO G, ENRIQUEZ, OSCAR R, BRUNET, PHILIPPE, COLINET, PIERRE & SNOELJER, JACCO H 2014 Universality of tip singularity formation in freezing water drops. *Physical review letters* **113** (5), 054301.
- RIVETTI, MARCO, SALEZ, THOMAS, BENZAQUEN, MICHAEL, RAPHAËL, ELIE & BÄUMCHEN, OLIVER 2015 Universal contact-line dynamics at the nanoscale. *Soft Matter* **11** (48), 9247–9253.
- DE RUITER, JOLET, SOTO, DAN & VARANASI, KRIPA K 2018 Self-peeling of impacting droplets. *Nature Physics* **14** (1), 35.
- SCHIAFFINO, STEFANO & SONIN, AIN A. 1997 Motion and arrest of a molten contact line on a cold surface: An experimental study. *Physics of Fluids* **9** (8), 2217–2226.
- SCHREMB, M., ROISMAN, I.V. & TROPEA, C. 2018 Normal impact of supercooled water drops onto a smooth ice surface: experiments and modelling. *J. Fluid Mech.* **835**, 1087–1107.
- SNOELJER, JACCO H & BRUNET, PHILIPPE 2012 Pointy ice-drops: How water freezes into a singular shape. *American Journal of Physics* **80** (9), 764–771.
- STEFAN, J. 1891 Über die theorie der eisbildung, insbesondere über die eisbildung im polarmeere. *Ann. Physik Chemie* **42**, 269–286.
- VIDAURRE, G. & HALLETT, J. 2009 Particle impact and breakup in aircraft measurement. *J. Atmos. Ocean. Technol.* **26**, 972–983.
- WILDEMAN, S., STERL, S., SUN, C. & LOHSE, D. 2017 Fast dynamics of water droplets freezing from the outside in. *Phys. Rev. Lett.* **118**, 084101.
- WORSTER, M.G. 2000 *Perspectives in Fluid Dynamics — a Collective Introduction to Current Research*, chap. Solidification of Fluids. Cambridge Univ. Press.